Front. Earth Sci. 2021, 15(1): 106–120
https://doi.org/10.1007/s11707-020-0853-x

RESEARCH ARTICLE

Identifying porphyry-Cu geochemical footprints using local neighborhood statistics in Baft area, Iran

Saeid GHASEMZADEH[1], Abbas MAGHSOUDI (✉)[1], Mahyar YOUSEFI[2]

1 Department of Mining and Metallurgical Engineering, Amirkabir University of Technology, Tehran 95799-79167, Iran
2 Faculty of Engineering, Malayer University, Malayer 65719-95863, Iran

Abstract Identifying geochemical anomalies related to ore deposition processes facilitates the practice of vectoring toward undiscovered mineral deposit sites. In district-scale exploration studies, analysis of dispersion patterns of ore-forming elements results in more-reliable targets. Therefore, deriving significant geochemical footprints and mapping the ensuing geochemical anomalies are of important issues that lead exploration geologists toward anomaly sources, e.g., mineralization. This paper aims to examine the effectiveness of local relative enrichment index and singularity mapping technique, as two methods of local neighborhood statistics, in the delineation of anomalous areas for further exploration. A data set of element contents obtained from stream sediment samples in Baft area, Iran, therefore was applied to illustrate the procedure proposed. The close relationship between anomalous patterns recognized and known Cu-occurrences demonstrated that the procedures proposed can efficiently model complex dispersion patterns of geochemical anomalies in the study area. The results showed that singularity mapping method is a better technique, compared to local relative enrichment index, to delineate targets for follow-up exploration in the area. We made this comparison because, as pointed out by exploration geochemists, dispersion patterns of geochemical indicators in stream sediments vary in different areas even for the same deposit type. The variety in the dispersion patterns is due to the operation of post-mineralization subsystems, which are affected by local factors such as landscape of the areas under study. Therefore, the effectiveness of the methods should be evaluated in every area for every targeted deposit.

Received January 20, 2020; accepted November 19, 2020

E-mail: a.maghsoudi@aut.ac.ir

Keywords local neighborhood statistics, robust principal component analysis, singularity mapping technique, local relative enrichment index, exploration targets

1 Introduction

Recognizing geochemical anomalies resulting from geological evolution and the related ore-formation processes (Cheng, 2007) is an important step toward undiscovered mineral deposit sites. From regional to district scale exploration targeting, the anomaly concept is defined as abnormal element concentrations in areas where there may be a link between the anomalous concentrations and the corresponding ore deposition processes, which could vector us to mineral trap sites (Cheng, 2007; Cheng and Agterberg, 2009; Zhao et al., 2012; Zuo, 2014; Zhao et al., 2016; Wang et al., 2017; Zhou et al., 2018; Yousefi et al., 2019). Therefore, better and more-precise identification of the geochemical anomalies facilitate the delineation of exploration targets (e.g., Grunsky et al., 2009; Zuo, 2011; Yousefi, 2017a; Parsa et al., 2018a). Stream sediment geochemical studies are well-known and widely-used methods for district scale mineral exploration targeting (e.g., Cheng, 2007; Carranza, 2011; Ghasemzadeh et al., 2019a; Yu et al., 2019; Afzal et al., 2019). Materials of stream sediment samples are products of erosion and weathering processes affected by many local factors (Macklin et al., 1994; Spadoni et al., 2005; Spadoni, 2006; Yousefi et al., 2013) so that chemical contents of such samples are related to upstream rock types and the corresponding sources (Moon, 1999; Spadoni, 2006; Xie et al., 2010; Yousefi et al., 2013, Parsa et al., 2016). Complexities in the erosion and weathering processes, operating as post-mineralization subsystems (Yousefi et al., 2019) to exhume mineral deposits and their dependency to local characteristics of the area under prospecting, make the interpretation of geochemical data a

difficult undertaking (Chaffee et al., 1981; John et al., 2010). Furthermore, spatial distribution patterns of mineralization-related indicator elements are affected by physical and chemical characteristics of the elements (e.g., mobility) as well. Thus, the anomalous contents of indicator elements do not locate in the same positions downstream of deposit sites (Yilmaz, 2003a; Cheng, 2007; Zuo et al., 2009a; Xie et al., 2010; Yousefi et al., 2013; Parsa et al., 2016), which make it difficult to discover anomaly sources. In this regard, there are two general approaches for geochemical anomaly delineation, namely frequency and spatial methods (e.g., Zuo et al., 2013; Zuo, 2014). The former approaches, e.g., classical statistical methods and conventional multivariate data analysis tools (Reimann et al., 2002; Cheng et al., 2006; Zuo, 2011; Yousefi et al., 2012), do not take into account the spatial characteristics of geochemical data, and use only the frequency characteristics of element contents to identify geochemical anomalies (Zuo et al., 2013; Zuo, 2014; Zuo and Wang, 2016; Ghasemzadeh et al., 2019a). In contrast the latter methods, e.g., spatial U-statistics (Cheng et al., 1996; Cheng, 1999), concentration-area (Cheng et al., 1994), power spectrum-area (Cheng et al., 2000), singularity mapping technique or local singularity analysis (SM) (Cheng, 2007), and Local relative enrichment index (LREI) (Zuo, 2014), simultaneously consider frequency and spatial properties of geochemical data and their self-similarity. Furthermore, various machine learning algorithms such as continuous restricted Boltzmann machine (Chen et al., 2014), quantile regression forests (Kirkwood et al., 2016), maximum margin metric learning algorithm (Wang et al., 2019), and a combination of deep learning and support vector machine (Xiong and Zuo, 2020) have been widely used in geochemical anomaly mapping. These methods are not sensitive to the negative effect of outliers and the statistical distribution of the data (e.g., Zuo, 2017; Wang et al., 2019). Further discussions about machine learning algorithms are found in Zuo (2017).

The aims of this paper are 1) to derive strong and significant multivariate geochemical signatures of mineral deposit of the type sought through robust principle component analysis (RPCA), 2) to model the corresponding geochemical anomalies by using both SM and LREI techniques as local neighborhood statistics approaches, and 3) to compare the modeling results for the purpose of introducing more-reliable exploration targets. To illustrate the procedures applied and to demonstrate their effectiveness in the delineation of exploration targets, a data set of element contents in stream sediment samples of Baft district, south-eastern Iran was applied for prospecting porphyry-Cu deposits.

2 Deposit model and the study area

The favorable properties of porphyry-Cu deposits (their large size, long mine lives and high production rates) have made them as a world's most important source of Cu and Mo (John et al., 2010). These deposits are also important sources of other economic metals like Au and Ag (Sillitoe, 1972, 2010). These deposit types are the end product of post magmatic hydrothermal fluids and are spatially and genetically associated with intrusive rocks commonly forming in the upper crust (less than 5–10 km depth) (Sillitoe, 1972, 2010; Singer et al., 2005). The intrusive rocks with dioritic to granitic compositions, for instance quartz monzonite, diorite, granodiorite, quartz diorite, and monzonite are heat sources for this type of mineralization (Hezarkhani, 2006; Boomeri et al., 2009; Peytcheva et al., 2009). Hydrothermal alteration features such as potassic, sericitic, advanced argillic, intermediate argillic, propylitic, sodic-calcic and sodic, greisen, and skarn tend to be associated with this deposit type and show distinctive lateral and vertical zoning patterns (Sillitoe, 2010). Tectonic activities play an important role in the formation of porphyry-Cu deposits. They provide spaces for migration of the ore-bearing fluids and facilitate their circulation (e.g., Pirajno, 2010). In addition to the aforementioned geological aspects, porphyry-Cu deposits possess some geochemical characteristics representing the operation of some of the corresponding ore-forming chemical processes (Sillitoe, 2010; John et al., 2010). Therefore, understanding and translation of the processes into mappable exploration criteria through the geochemical data analysis are fundamental tasks in mineral exploration practices that help to find undiscovered mineral deposits sites (e.g., Zhao et al., 2012; Wang et al., 2020).

The Urumieh-Dokhtar magmatic arc (UDMA) of Iran (Fig. 1(a)), as a component of Alpine-Himalayan orogenic belt which was formed in association with closure of the Neotethyan Ocean in the Late Cretaceous (Mohajjel and Fergusson, 2000; Agard et al., 2007; Rezaei-Kahkhaei et al., 2011), is well known as one of the most important metallogenic belts in the world for exploration of subduction-related mineralization (e.g., porphyry-Cu deposits) (Hezarkhani and Williams-Jones, 1998; Hezarkhani, 2006; Zarasvandi et al., 2015). Reports and investigations carried out by many authors indicates that the majority of the known porphyry systems and prospects of Iran such as Sar cheshmeh, Songun, Meiduk, Kahang, Darezar, Darreh-Zerreshk, Dalli and Chah-Mesi have been distributed in this belt (Hezarkhani, 2006; Shafiei et al., 2009; Afzal et al., 2012; Ayati et al., 2013; Aghazadeh et al., 2015; Zarasvandi et al., 2015; Parsa et al., 2018b; Aliyari et al., 2020). The UDMA, of which the Baft district with a surface of about 1250 km^2 covers the study area of this paper, is the main Cu-endowed region of Iran (Shafiei et al., 2009; Mirzaie et al., 2015). This belt contains several known porphyry copper deposits such as Sarcheshmeh, Meiduk, Iju, Daraloo, Parkam (Sara), and many smaller and sub-economic reserves. A simplified geological map of the area is shown in Fig. 1(b). The volcanic rocks consist

of mainly andesite, andesite-basalt, dacite, and minor amounts of basalt and rhyolite of Eocene age widespread in north-east of the study area. These volcanic rocks were affected by Miocene intrusive bodies, the so-called the Lalezar granitoid (Niktabar et al., 2015) or Rabor – Lalehzar magmatic complex arc (RLMC) (Moghadam et al., 2018). These Jebale-Barez type granitoids (Dimitrijevic, 1973; Shafiei, 2010) have a range from gabbro-diorites to granites in composition (Srdic et al., 1972; Dimitrijevic, 1973; Niktabar et al., 2015). The mineral compositions of the most felsic rocks are characterized by the abundances of Na-plagioclase, quartz, alkali feldspar, biotite and hornblende (Srdic et al., 1972; Dimitrijevic, 1973). In the gabbro-diorite rocks, plagioclase (Ca-rich), hornblende, biotite and clinopyroxene are the most common minerals (Srdic et al., 1972; Dimitrijevic, 1973). Geological and geochemical studies demonstrated that the Lalezar granitoids are mostly metaluminous (Srdic et al., 1972; Dimitrijevic, 1973). However, the most felsic members of the Lalezar granitoids (i.e., granites) attain slightly peraluminous compositions and have characteristics of high-K calc-alkaline rocks (Srdic et al., 1972; Dimitrijevic, 1973). According to the geochemical features of the Oligocene granitoid rocks (similar to Jebal Barez-type) in Rabor-Lalehzar region, these rocks were derived from the partial melting of thickened lower crust. As indicated in Fig. 1(b), the RLMC was emplaced into volcanic rocks of Eocene age through faults and other fractures that are conspicuous structures in study area. Presumably, these fractures could provide the pathway for migration of fluids and control the mineralization (Sillitoe, 2010; Pirajno, 2010; Yousefi, 2017a). The deposit types in the north part of Baft district are mainly porphyry and vein systems (Table1), for example Hararan and Laleh zar

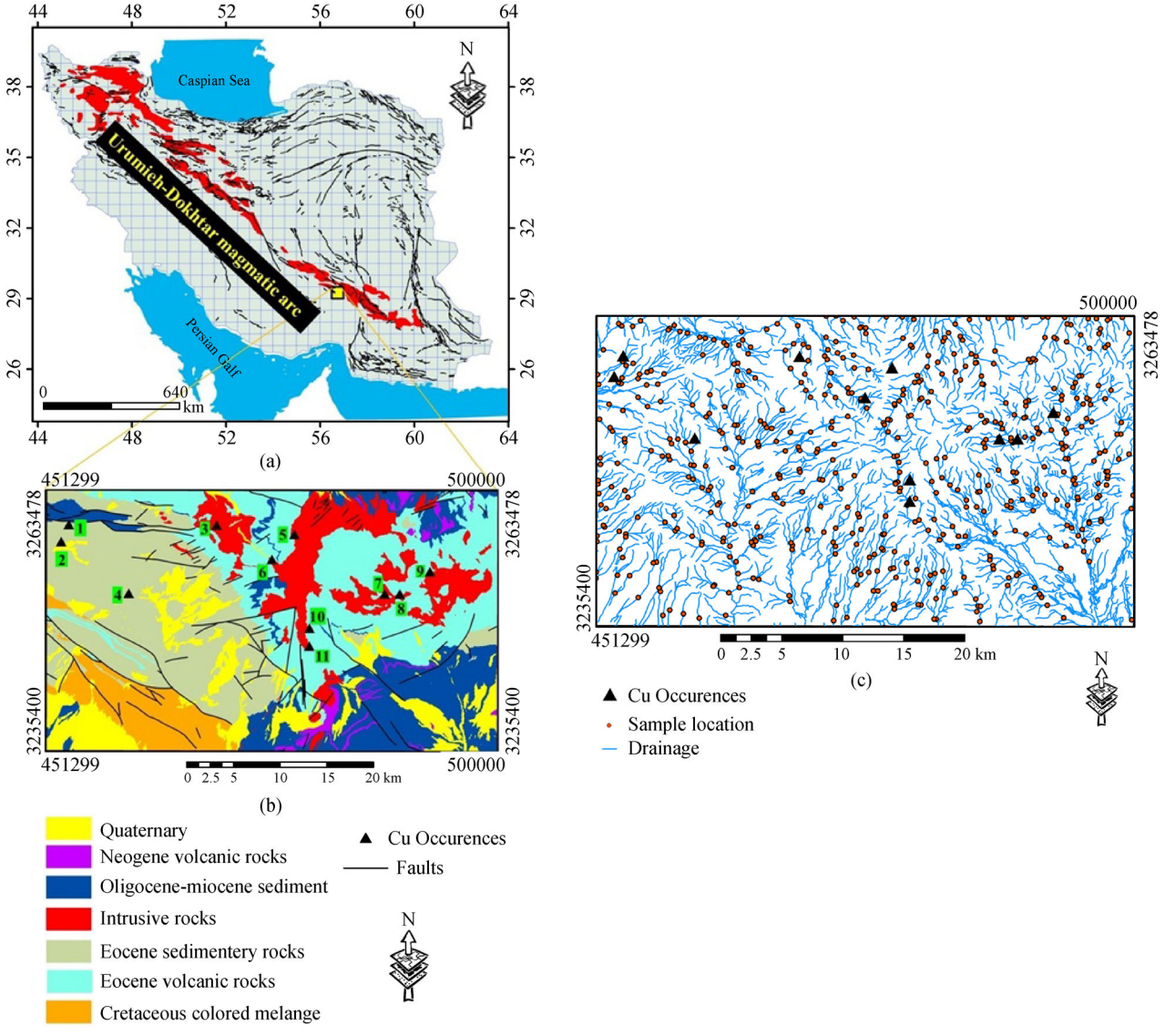

Fig. 1 (a) Urumieh-Dokhtar volcano-plutonic belt of Iran and location of the study area thereon, (b) Simplified geological map of the study area, and (c) The spatial distribution map of stream sediment samples.

Table 1 Cu-Occurrences of the study area (labeled in Fig. 1(b))

ID	Name	X	Y	Type
1	Goghar	453944	3259783	vein
2	Bid khan	453128	3257940	porphyry
3	Ghaleh Asghar	469834	3259730	porphyry
4	Ab Bahri	460382	3252372	vein
5	Ghaleh Asghar1	478182	3258726	porphyry
6	Harij(Hararan)	475752	3256022	porphyry
7	Lalezar2	487872	3252309	porphyry
8	Lalezar4	489489	3252308	porphyry
9	Paynegin	492724	3254706	vein
10	Lalezar	479780	3248628	porphyry
11	Lalezar3	479776	3246689	porphyry

porphyry deposits and Paynegin vein-type mineralization. As shown in the Table 1 the deposit (ID = 2) is porphyry type. Unpublished reports by the National Iranian Copper Industries Company (NICICO) indicate this deposit is associated with intrusive rocks. However, because of the map scale (1:100000), which covers vast area, the relevant intrusion (having a small dimension) has not been portrayed in the map (Fig. 1(b)). Vein-type deposits (e.g., ID = 9) are also formed in and around intrusive masses and their sources are in fact the intrusions. The porphyry-Cu deposits in the UDMA of Iran show geochemical halos of indicator elements mainly Cu, Mo, Au, Ag, Zn, Pb, As, and Sb (e.g., Yousefi et al. 2012; Ghasemzadeh et al., 2019a). Therefore, the spatial distributions of these associated elements in surface media such as stream sediments, soil and rocks can be used in exploring these deposits (e.g., Sillitoe, 2010).

In the study area, Eocene volcanics with andesite and latite-andesite composition intruded by the Upper Miocene quartz monzodiorite, granodiorite, monzonite, and Mio-Pliocene post-mineralization and dioritic dikes (Srdic et al., 1972; Jamali, 2017). The hydrothermal alterations mostly silica and locally argillic, have been developed within and surrounding of the intrusions (Shafiei et al. 2009; Jamali, 2017). Disseminated Cu-Fe mineralization, with anomalous amounts of Cu (up to 1300 mg/L) and Mo (up to 3 mg/L), formed as stock works, and sheeted veinlets of quartz, magnetite, and chalcopyrite within the Upper Miocene quartz monzodiorite and Eocene volcanics (Shafiei et al. 2009; Jamali, 2017).

3 Methods

3.1 Robust principal component analysis

Principal component analysis (PCA) has been widely used as a powerful multivariate analysis tool for dimension reduction and detection of hidden structure in multivariate geochemical data (Reimann et al., 2002; Cheng et al., 2006; Zuo, 2011; Xoia et al., 2020). PCA is an efficient method for generating multi-element geochemical signatures such that its application reveals the elemental association thereof, and so, improves our understanding about the underlying ore-forming geochemical processes (Jolliffe, 2002; Cheng et al., 2011; Zuo et al., 2013; Soltani et al., 2019).

The ordinary PCA is based on covariance (or variance) matrix, which is influenced by the outlier data. The outlier data can spoil the covariance structure and the estimation of principal components (PCs) (Filzmoser et al., 2009a). In addition, the resulting PC1 that contains useful information is often inclined toward the outlying data (e.g., Zuo et al., 2013). Therefore, the presence of outlier data causes the result of ordinary PCA become unreliable and unaccountable, and so, may not capture the variation of the regular observations (Reimann and Filzmoser, 2000; Filzmoser and Hron, 2008; Rocha et al., 2013). For modulating these shortcomings, an extension algorithm of PCA, the robust PCA (RPCA) (Filzmoser et al. 2009a), can be applied to achieve the correct inferences (Pison et al., 2003; Filzmoser and Hron, 2009; Wang and Zuo, 2015). The RPCA technique overcomes the negative effects of outlier by using minimum covariance determinant estimator (e.g., Rousseeuw and Driessen, 1999). However, it still has not been very successful because the compositional nature of geochemical data is not taken into account in the processing procedures. To improve the efficiency of RPCA, application of log-ratio transformation is arguably the best choice (Aitchison, 1986; Aitchison et al., 2000; Filzmoser and Hron, 2009; Filzmoser et al., 2009a; Buccianti, 2015; Buccianti et al., 2018; Darabi golestan and Hezarkhani, 2019). There are three types of log-ratio transformation, namely additive log-ratio (alr) (Aitchison, 1986), centered log-ratio transform (clr) (Aitchison, 1986), and the isometric log-ratio (ilr) (Egozcue et al., 2003) that

modulate the closure problems. Running RPCA on ilr-transformed geochemical data are effective framework for addressing the aforementioned PCA limitations and negative effects of closure problem (e.g., Filzmoser et al., 2009a). It should be noted here that ilr transformation does not yield a one-to-one transformation from simplex space to Euclidean space. Thus, for better interpretation, it is necessary to back the ilr-transformed data to clr space prior to running RPCA (Filzmoser et al., 2009a).

3.2 Singularity mapping technique

The identification of geochemical anomalies caused by mineralization is an essential exploration stage for delimiting exploration targets (e.g., Cheng, 2007; Zuo et al., 2009a; Yousefi et al., 2012; Zuo, 2014). It has been demonstrated that singularity is a crucial property inherent from ore-forming geological processes (e.g., Cheng, 2007; Cheng and Agterberg, 2009; Zuo et al., 2009a; Bai et al., 2010; Xiao et al., 2012, 2020; Zuo and Wang, 2016, Parsa et al., 2017a). From geological perspective, this significant property describes the underlying geological processes operating as throttle to form mineral deposits in trap sites through enrichment and abnormal accumulation of geochemical elements within a spatial–temporal interval (Cheng, 2007; Yousefi et al., 2019). Therefore, the quantitative estimation of singularity is an effective tool to provide complementary information for recognizing mineralization-related geochemical anomalies (Zuo et al., 2009a).

From a multi-fractal point of view, for a 2D modeling space, the singularity index (α) can be characterized through a power-law model as following (Cheng, 2007; Zuo et al., 2009a):

$$\mu(A) = cA^{\frac{\alpha}{2}}, \tag{1}$$

$$C(A) = cA^{\frac{\alpha}{2}-1}, \tag{2}$$

where for an area of size A, $\mu(A)$ and $C(A)$ are the total amount of metal and the average metal concentration, respectively, and c is constant. The $C(A)$ for the area A can be expressed as $C(A) = \mu(A)/A$. The index α can be estimated from the values $C(A)$, which is calculated for different sizes of A by means of least squares (LS) fitting of a straight line on log–log paper. For a 2D modeling practice (e.g., a geochemical distribution map), a value of $\alpha < 2$ for a certain location indicates abnormal enrichment of the element while a value of $\alpha > 2$ for a certain location indicate elemental depletion. In this regard, $\alpha \approx 2$ represents non-singularity. In the application for information extraction, the singularity index can be estimated using singularity mapping (SM) technique (e.g., Cheng, 2007; Zuo et al., 2009a; Zuo and Wang, 2016). This method is a version of concentration-area fractal modeling approach that calculates the value of singularity index through measuring the relative changes in elemental concentration using a window-based algorithm. General framework of a window-based SM algorithm for a 2D modeling includes the following steps (Cheng, 2007; Zuo et al., 2009a): 1) Defining a set of sliding windows $A(r)$ with variable window sizes so that $r_{\min} = r_1 < r_2 < \ldots < r_n = r_{\max}$. In this step, various shapes of window such as square, circular, rectangular annulus, circle, rectangle, and wedge can be used; however, a square form is predominant. The values of and are dependent on the resolution of the data and geological properties of the study area, respectively (Cheng, 2007). 2) Superimposing the defined set of windows on a certain location with a specific coordinates ($P(x, y)$), and calculating the average concentration $C[A(r_i)]$ per window with predefined cell size (r_i). 3) Estimating the singularity index value α for the location $P(x, y)$ through the following equation:

$$\log C[A(r_i)] = C + (\alpha - 2)\log(r_i). \tag{3}$$

4) Repeating the steps of 2 and 3 for other location of the 2D geochemical distribution map.

More comprehensive descriptions of singularity concept and singularity mapping technique can be found in Cheng (2007) and Zuo et al. (2009a).

3.3 Local relative enrichment index (*LREI*)

The local neighborhood statistics are robust methods for revealing local information about geochemical data structure and identifying geochemical anomalies related to mineralization events of certain types (Zhang et al., 2007; Zuo, 2014). They explore the spatial variations of geochemical patterns and reduce the effects of geochemical background by considering only data within the small neighborhood around specific locations, e.g., mineral deposit sites (Zhang et al., 2007; Zuo, 2014; Wang and Zuo, 2016).

LREI is a type of robust neighborhood statistic (Zuo, 2014), which can be considered as a kind of soft threshold method to examine the spatial variation of elemental concentrations in a small neighborhood based on the sliding window technique (Zuo, 2014; Zhou et al., 2015). *LREI* is a powerful tool for the delineation of geochemical anomalies in regional scale exploration programs. It can reduce the negative effects of regional background on anomaly identification in complex geological settings as well (Zuo, 2014; Wang and Zuo, 2016).The *LREI* for a location z_i is expressed as (Zuo, 2014):

$$LREI(z_i) = \frac{X_i - \mathrm{MEDEAN}_i}{\mathrm{MEDEAN}_i} = \frac{X_i}{\mathrm{MEDEAN}_i} - 1, \tag{4}$$

where X_i is the concentration of geochemical element (i.e., element content) at the location z_i and MEDIAN_i is the median value of the element in a specific small neighboring cells around z_i.

4 Results

4.1 Data set and pre-processing

Anomalous contents of Cu, Mo, Zn, Pb, Ag, As and Sb elements are genetically related to porphyry-Cu mineralization (Yilmaz, 2003b; Halter et al., 2004; Singer et al., 2005; Qu et al., 2007; Yang et al., 2009; Yousefi et al., 2012; Parsa et al., 2016; Afzal et al., 2016; Yousefi, 2017a, 2007b; Ghasemzadeh et al., 2019b). Therefore, recognizing abnormal dispersion patterns of these elements in spatial is a vector toward mineralization sites. To recognize mineralization-related geochemical anomalies, a data set of 535 stream sediment samples, collected, prepared, and analyzed by geological survey of Iran with a sampling density of one sample per 4 km^2, was used in this study (Fig. 1(c)). The inductively coupled plasma-optical emission spectrometry (ICP-OES) method was employed to analysis the concentration values of Cu, Mo, Zn, Pb, As and Sb. The detection limits of Cu, Mo, Zn, Pb, As, and Sb are 1, 0.5, 1, 1, 0.5, and 0.5, respectively. The values of all elements are in ppm. Precision of the analysis was estimated based on Thompson and Howarth (1976) method. The results indicated that the precision was better than 10% for most of the elements, so the concentration values are suitable for further interpretation steps. As Reimann et al. (2002), Zuo et al. (2009a), Zuo (2011), and Zhao et al. (2016) pointed out, understanding of the nature of geochemical data (e.g., normal or log-normal) is required prior to the data processing for delineation of geochemical anomalies. This is because selection of an efficient method for geochemical anomaly identification is depended on the type of distribution of the geochemical data (Reimann and Filzmoser, 2000; Zheng et al., 2014; Xiong et al., 2018). According to Allègre and Lewin (1995), geochemical data distributions can be categorized into two general groups: normal and multimodal distributions and fractal and multifractal distributions (Gong et al., 2018). In the present study, to determine distribution types of stream sediment data, "quantile–quantile" (Q–Q) plot and skewness parameter were used. The summary of statistical information of the indicator elements are presented in Table 2. From the skewness and the Q–Q plots of log-transformed elemental concentration values (Fig. 2) it can be concluded that concentration values of the elements do not follow either a normal or a lognormal distribution (Cheng et al., 1994; Zuo, 2011; Xiao et al., 2012; Zhao et al., 2016). Therefore, the study area has been influenced by multiple geological events or processes that have operated over a variety of geological time and scales (Reimann et al., 2002; Zuo et al., 2009a; Zuo, 2011).

4.2 Deriving significant multi-element geochemical footprint

In this study, to calibrate the negative influences of outliers and the closure problems thereof and to reveal elemental associations for deriving a desirable multi-element geochemical signature, the following steps were taken in R free software (Templ et al., 2011): 1) The ilr transformation was applied on raw geochemical data (i.e., concentration values of Cu, Mo, As, Sb, Zn, Pb) (Filzmoser et al. 2009a and 2009b); 2) The RPCA was performed on the ilr-transformed data, and the results obtained revealed that most of the data variability (33.06%) are explained in the first robust principal component (RPC1). The second robust principal component explains (RPC2) 13.85% of the data variability. Therefore, the two first components account 46.91% of the total variance of the data set. Thus, this variability is acceptable; 3) the loadings obtained and the scores calculated were transformed back to clr-space (Filzmoser et al., 2009aand 2009b; Zuo, 2014; Wang and Zuo, 2015); 4) the clr-transformed loadings and scores of RPC1 and RPC2 were presented through compositional biplot (Fig. 3(a)). As Fig. 3(a) demonstrates, the RPC1 reflects an association of Cu, Mo and Zn elements. In the other words, these elements show positive loadings in RPC1. Given that these elements have genetic and spatial relationships with porphyry-Cu deposits (Yilmaz, 2003b; Halter et al., 2004; Singer et al., 2005; Xiaoming et al.,

Table 2 The statistical parameters of porphyry-Cu indicators.

	Cu	Mo	Au	Ag	As	Sb	Zn	Pb
Mean	68.53	1.13	0.00	0.21	25.25	2.37	125.14	69.29
Median	62.70	0.89	0.00	0.10	17.70	1.22	90.00	15.60
Std. deviation	26.48	0.74	0.01	1.34	36.32	6.21	292.55	519.08
Maximum	331.00	6.96	0.25	29.40	743.00	119.00	5640.00	10000.00
Minimum	24.00	0.50	0.00	0.10	2.40	0.50	51.00	4.40
Mode	66.50	0.56	0.00	0.10	13.80	0.54	85.00	9.90
Skewness	3.08	3.44	12.15	19.85	14.86	13.74	14.85	15.25
Kurtosis	20.37	16.60	193.60	422.30	283.88	236.88	252.21	264.43
25th Percentile	52.80	0.71	0.00	0.10	12.40	0.73	80.00	11.75
75th Percentile	77.60	1.29	0.00	0.10	30.20	2.29	108.00	23.20

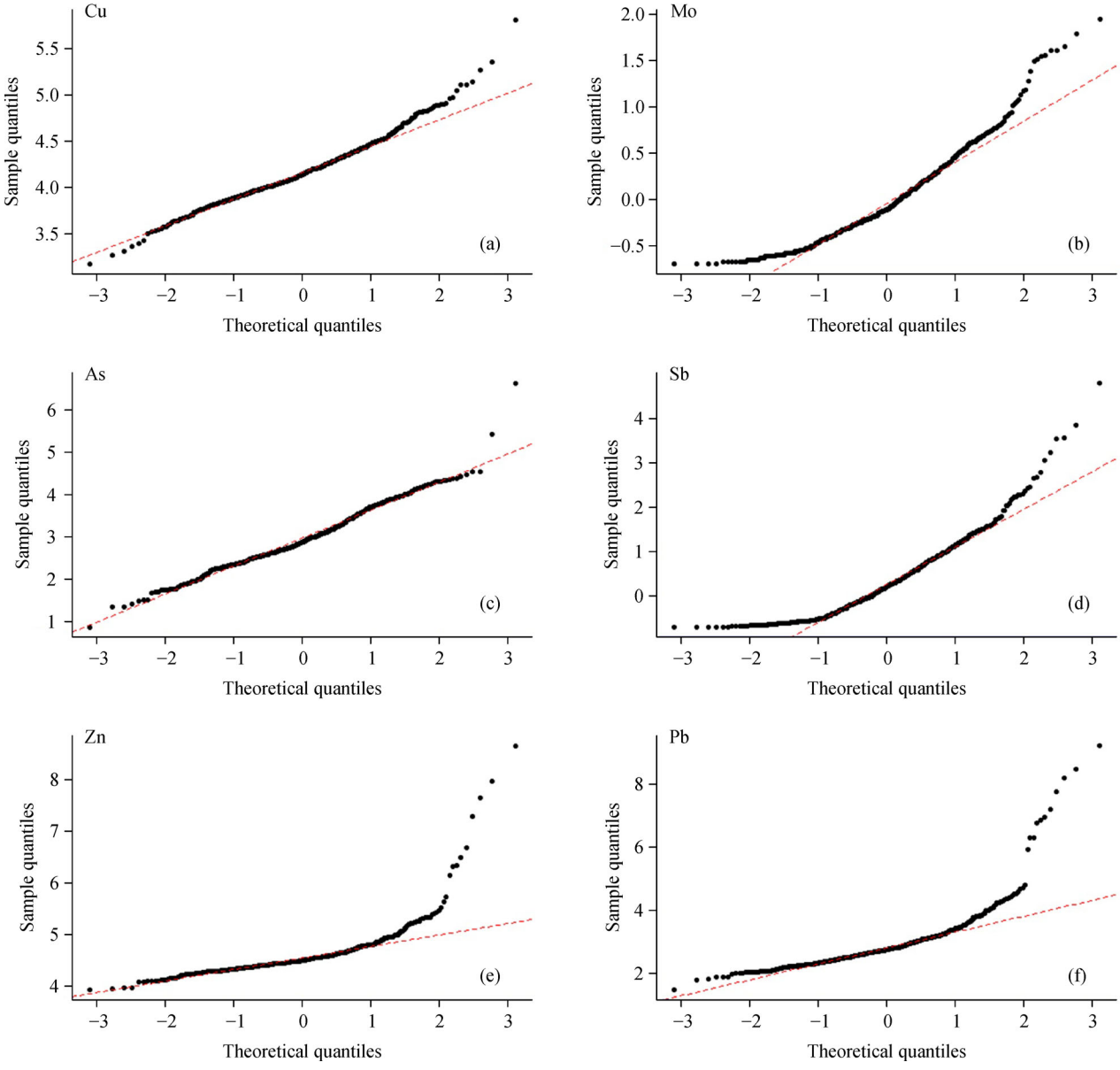

Fig. 2 Q-Q plot of (a) Cu, (b) Mo, (c) As, (d) Sb, (e) Zn, (f) Pb elements studied.

2007; Yang et al., 2009; Yousefi et al., 2012; Parsa et al., 2016; Yousefi, 2017b) and inflection point of the scree plot appeared at principal component number 1 (Fig. 3(b)), RPC1 can be applied as a significant multi-element signature for prospecting the targeted deposit type in the study area.

The rescaled range statistic (*R*/*S*) (Mandelbrot and Wallis, 1969) was used to estimate the Hurst exponent (Hurst, 1951) for characterizing the distribution of RPC1 scores in the study area. The Hurst exponent is estimated by measuring the slope of a straight line on the log-log plot of *R*/*S* against the sample number (Fig. 4). The Hurst exponent for score of RPC1 with high goodness of fit (e.g., *R* squaregreater than 0.97) is > 0.77 (Fig. 4). The calculated Hurst exponent represents persistent phenomena and heterogeneous distribution of RPC1scores in study area because it is greater than 0.5 (Zuo et al., 2009b).

4.3 Mapping anomalies using *LREI* and SM techniques

After deriving multivariate geochemical signatures, selecting appropriate anomaly mapping methods and their discrimination from background are challenging confrontation in the context of geochemical data processing (Harris et al., 2000; Zuo, 2011; Zhao et al., 2016). It should be noted here that in order to estimate the *LREI* values, a suitable window size must be selected, which could be different with the sampling cell size (e.g., Carranza, 2009).

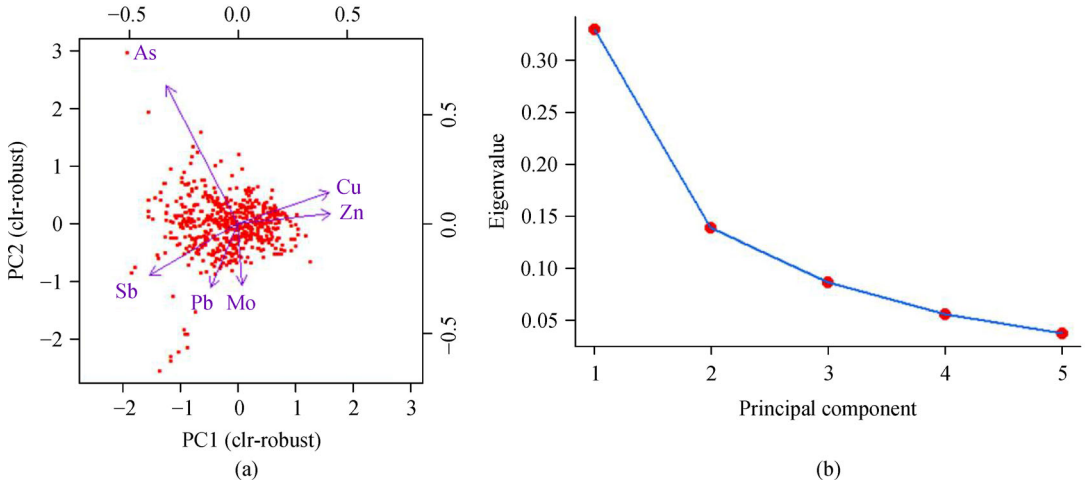

Fig. 3 (a) The ore-forming elements biplot of RPC1 agnaist RPC2 of ilr- transformed data, and (b) extracted scree plot of RPCA.

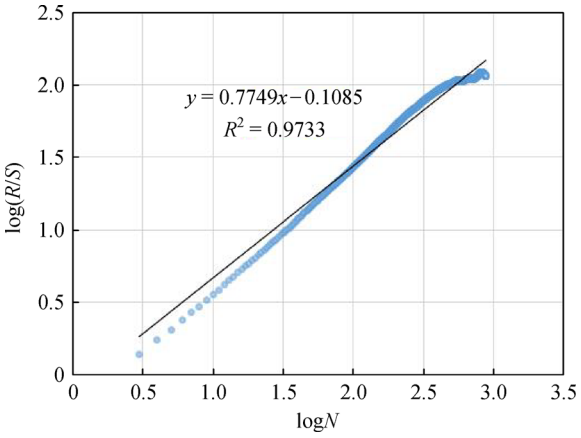

Fig. 4 log–log plots of (*R*/*S*) versus the number of sample in the study area.

An optimal window size can be defined based on spatial dependency through variogram analysis (Tian et al., 2018; Ghasemzadeh et al., 2019a). In this paper, a square window size of 5 km × 5 km was obtained and applied to calculate *LREI* of Cu, Mo, As, Sb, Zn and Pb. Then, the values of *LREI* were transformed into logistic space, [0, 1] range, by the Eq. (1) of Yousefi and Carranza (2015). Subsequently, logistically-transformed LREI values were integrated by fuzzy gamma operator with a gamma value of 0.97. Figure 5 illustrates the classified distribution map of integrated local relative enrichment index of indicator elements using fuzzy gamma operator.

For further analysis and evaluation of the effectiveness of the SM technique in terms of recognizing the mineralization-related geochemical anomalies, a cell size of 350 m × 350 m was used for gridding the RPC1 scores into a raster map (Fig. 6). Density of samples, mapping scale, and the structure of point patterns are of criteria for choosing a suitable cell size (Hengl 2006; Zuo 2012; Zhou et al., 2015). In this study, the structure of point patterns was used for selection of the proper above-mentioned grid size as pointed out by Zhou et al., (2015). Then, a set of square sliding windows with variable sizes of 1050 m × 1050 m, 1750 m × 1750 m, ..., and 5250 m × 5250 m were defined. These sizes were multiples of the initial cell size (i.e., 350 m). The average element concentration per window, defined cell size, was calculated first. Then the corresponding singularity index was calculated using least squares fitting according to Eq. (3).) Finally, the IDW method was applied to interpolate the values of singularity index (Fig. 7).

To quantitatively compare and evaluate the performance of the methods and to select an effective model of geochemical anomalies, we applied the success-rate curve (Fig. 8) (Agterberg and Bonham-Carter, 2005). A success-rate curve can be generated based on two parameters. One is proportion of mineral occurrences predicted correctly, which is plotted on Y-axis. The other is proportion of the study area classified as prospective, which is plotted on X-axis (Agterberg and Bonham-Carter, 2005). A diagonal line on the plot of the success-rate curve is a gauge line and plays an important role (Parsa et al., 2016 and 2017b). As a general rule, if the success-rate curve of a geochemical model appears above the gauge line, it can be inferred that the method is reliable. If the success-rate curve of a method appears higher in comparison with another method, it means that the former has performed over the latter. As Fig. 8 shows, the curves of the both methods appear above the gauge line, indicating the usefulness of the methods applied for identifying geochemical anomalies, however, SM technique is superior.

5 Discussion

Recognition of significant geochemical footprints of ore deposition processes and modeling their dispersion patterns are of important issues (Cheng, 1999; Zuo,

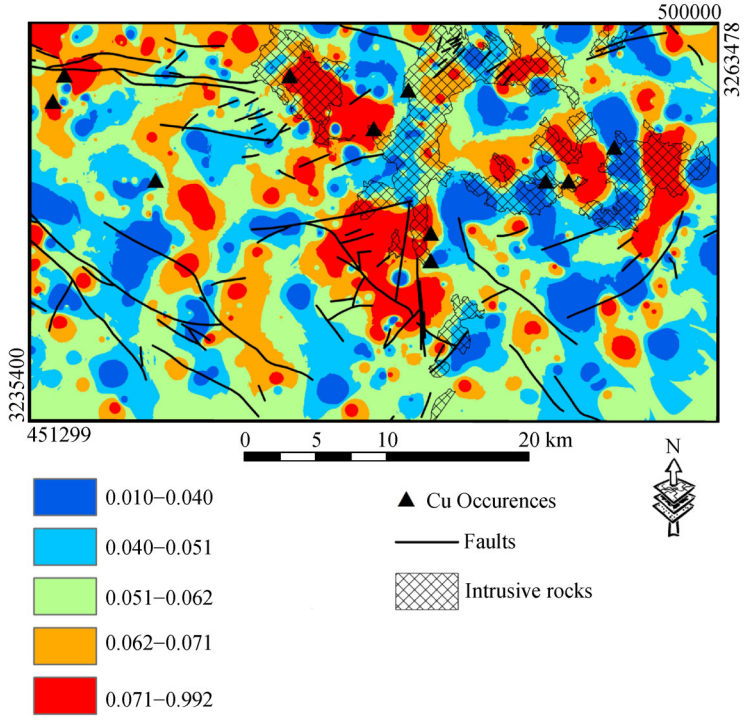

Fig. 5 Distribution map of integrated local relative enrichment index of ore-forming elements using fuzzy Gamma operator.

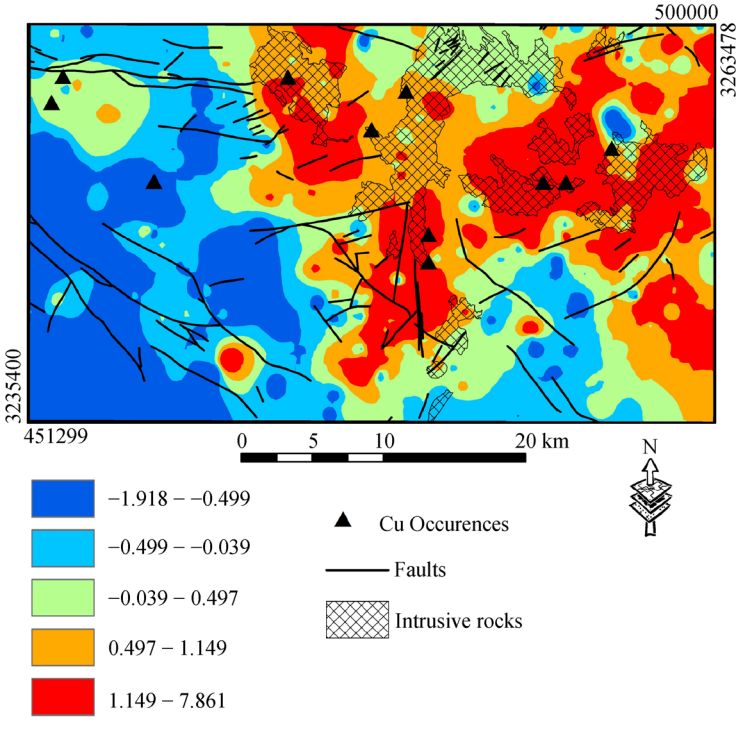

Fig. 6 The spatial distribution map of the multivariate geochemical signatures (RPC1 scores).

2011; Zuo and Wang, 2016) for vectoring toward undiscovered mineralized zones in a more-precise way (Xie et al., 2008; Grunsky et al., 2009; Cohen et al., 2010; Wang et al., 2015; Yousefi, 2017a, b; Parsa et al., 2018b; Ghasemzadeh et al., 2019a, b). In preliminary to intermediate scales of mineral exploration targeting (for

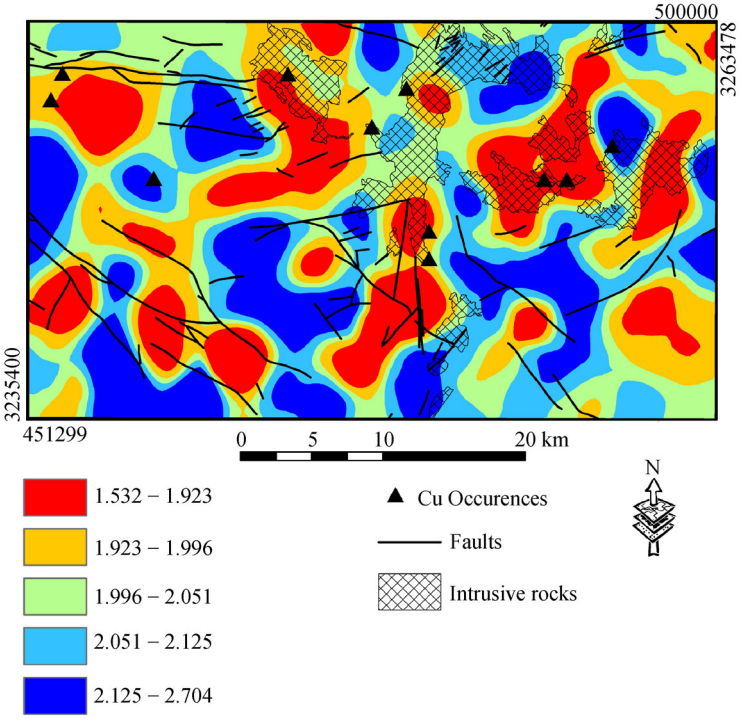

Fig. 7 Distribution map of local singularity index of RPC1 scores.

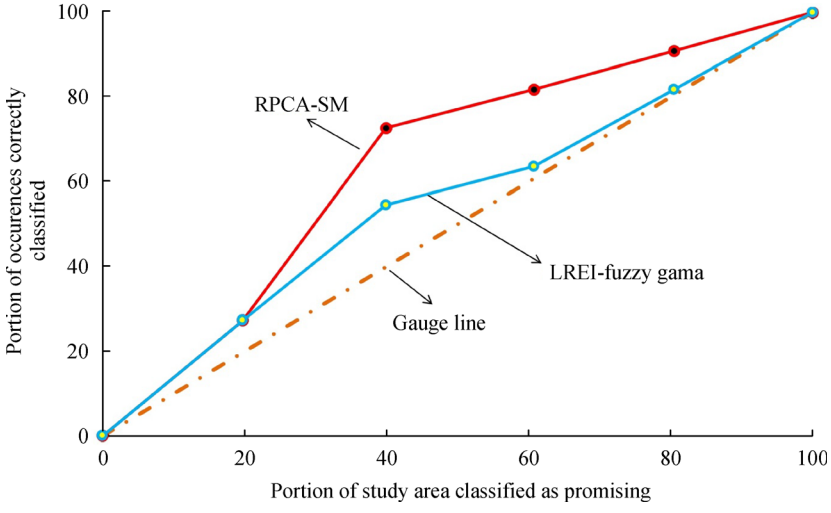

Fig. 8 Success-rate curves of the LERI-fuzzy and SM-RPCA techniques.

example here district-scale), data sets of element contents in stream sediments are commonly used to identify features, which are responses to the operation of geochemical ore-forming processes (Carranza and Hale, 1997; Carranza, 2008; Zuo et al., 2009a; Bai et al., 2010; Zheng et al., 2014; Yousefi and Nykänen, 2017; Yousefi et al., 2019; Kreuzer et al., 2020). Because of differences in physical and chemical characteristics (e.g., mobility) of geochemical elements, stream sediment samples with anomalous concentrations of different indicator elements can be located differently downstream of an anomaly source (Yilmaz, 2003a; Cheng, 2007; Zuo et al., 2009a; Xie et al., 2010; Yousefi et al., 2013; Parsa et al., 2016). In this regard, surficial geochemical patterns of indicator elements even for a certain type of mineral deposit vary in different areas. Therefore, in the distribution maps of different geochemical signatures of a certain deposit-type sought, geochemical anomalies may or may not coincide (Carranza, 2008; Yousefi, 2017a, 2017b). Accordingly, it is important to integrate different geochemical signatures of

the deposit to make a stronger indicator (Carranza, 2008; Yousefi et al., 2012; Parsa et al., 2016, Yousefi, 2017a; Zuo and Xiong, 2020). Consequently, a significant multi-element geochemical signature refers to a derived geochemical clue that has high ability in delimiting exploration targets for vectoring toward undiscovered mineral deposits.

Due to difficulty in the definition of influence area of stream sediment samples, which their spatially-distributed materials come from the entire upstream of the samples (Bonham-Carter, 1994; Carranza and Hale, 1997; Spadoni, 2006; Carranza, 2008; Yilmaz, 2003b; Yousefi et al., 2013), deriving significant mineralization-related footprints are major concerns as well (Cheng, 2007; Zuo and Wang, 2016). Therefore, effective methods are required to adequately convert geochemical data into information about their underlying structures. Subsequently, gaining knowledge about the possible spatial and genetic relationships between mineralization and indicator elements (i.e., elemental association and their distribution patterns) are facilitated (Yousefi et al., 2019; Zuo and Xiong, 2020). In the study area of this paper, the strong spatial relationship between multivariate geochemical signature (RPC1 scores) and the locations of known mineralization indicates that RPCA results are reliable to be used for gaining knowledge about the underlying elemental associations.

Finding and application of an efficient geochemical anomaly mapping method to address the transported nature of stream sediment geochemical anomalies are important challenging tasks in geochemical exploration (Cheng, 2007; Yousefi et al., 2013; Zuo, 2014). In this regard, hard threshold techniques ignore spatial variability of the elemental concentration (Cheng et al., 1994 and 1996; Li et al., 2003; Zuo et al., 2009a; Afzal et al., 2010) and only specify an overall threshold in a study area (Zhou et al., 2015). Thus, they are useful only for areas where the geochemical data follow normal distribution (Reimann and Filzmoser, 2000; Andrada de Palomera et al., 2015; He et al., 2013). This caveat adversely affects precise definition of geochemical anomalies, especially in the interpretation process of stream sediment data, in which the materials of the samples are spatially distributed (Bonham-Carter, 1994; Carranza and Hale, 1997) and generally show complex patterns (Macklin et al., 1994; Spadoni, 2006; Zuo et al., 2009a; Yousefi et al., 2013). In contrast, SM and LREI (Zuo, 2014; Wang and Zuo, 2016), as two special types of local neighborhood statistics and soft threshold techniques, are efficient to be used for the identification of anomalies in areas with complex geochemical data structure.

In this paper, the superiority of SM over *LREI* technique was demonstrated for extracting geochemical anomalies related to ore deposition processes in the area studied. However, further works and discussions, dealing with various aspects of mathematical foundation, geological application, and theoretical support, are needed to evaluate the ability of SM and *LRE* in different geochemical landscapes and to improve their effectiveness.

6 Conclusions

The findings of this study could be summarized as below:

- The significant geochemical evidence layer, generated in this study, is in fact a spatial proxy representing the underlying ore deposition processes and that model can be integrated with other exploration data to define targets.
- Higher effectiveness of the singularity mapping technique, compared to local relative enrichment index, has been demonstrated for identifying weak geochemical anomalies in the study area of this paper. Consequently, that anomalous areas delineated by singularity mapping technique can be used as exploration targets for follow-up exploration.
- The close relationship between deposit locations and the exploration evidence features (i.e., geochemical anomalous pattern identified by the subsequence use of robust principal component analysis and singularity mapping technique, conspicuous structures, and intrusive rocks) indicates that the geochemical anomalies are credible, and thus, the ensuing exploration targets can be planned for further exploration.

Acknowledgements The authors thank editor-in-chief and associate editors for journal of Frontiers of Earth Science for handling this work. The authors would thank five anonymous reviewers for their constructive comments and suggestions.

References

Afzal P, Khakzad A, Moarefvand P, Omran N R, Esfandiari B, Alghalandis Y F (2010). Geochemical anomaly separation by multifractal modeling in Kahang (Gor Gor) porphyry system, Central Iran. J Geochem Explor, 104(1–2): 34–46

Afzal P, Alghalandis Y F, Moarefvand P, Omran N R, Haroni H A (2012). Application of power-spectrum–volume fractal method for detecting hypogene, supergene enrichment, leached and barren zones in Kahang Cu porphyry deposit, Central Iran. J Geochem Explor, 112: 131–138

Afzal P, Mirzaei M, Yousefi M, Adib A, Khalajmasoumi M, Zia Zarifi A, Foster P, Yasrebi A B (2016). Delineation of geochemical anomalies based on stream sediment data utilizing fractal modeling and staged factor analysis. J Afr Earth Sci, 119: 139–149

Afzal P, Yousefi M, Mirzaie M, Ghadiri-Sufi E, Ghasemzadeh S, Daneshvar Saein L (2019). Delineation of podiform-type chromite mineralization using geochemical mineralization prospectivity index and staged factor analysis in Balvard area (SE Iran). J Min Environ, 10(3): 705–715

Aghazadeh M, Hou Z, Badrzadeh Z, Zhou L (2015). Temporal–spatial distribution and tectonic setting of porphyry copper deposits in Iran: constraints from zircon U–Pb and molybdenite Re–Os geochronology. Ore Geol Rev, 70: 385–406

Agard P, Jolivet L, Vrielynck B, Burov E, Monie P (2007). Plate acceleration: the obduction trigger? Earth Planet Sci Lett, 258(3–4): 428–441

Agterberg F P, Bonham-Carter G F (2005). Measuring the performance of mineral-potential maps. Nat Resour Res, 14(1): 1–17

Aitchison J (1986). The Statistical Analysis of Compositional Data. London: Chapman and Hall.

Aitchison J, Barcelo-Vidal C, Martín-Fernandez J, Pawlowsky-Glahn V (2000). Logratio analysis and compositional distance. Math Geol, 32 (3): 271–275

Allègre J C, Lewin E (1995). Scaling laws and geochemical distributions. Earth Planet Sci Lett, 132(1–4): 1–13

Aliyari F, Afzal P, Harati H, Zengqian H (2020). Geology, mineralogy, ore fluid characteristics, and $^{40}Ar/^{39}Ar$ geochronology of the Kahang Cu-(Mo) porphyry deposit, Urumieh-Dokhtar Magmatic Arc, Central Iran. Ore Geol Rev, 116: 103238

Ayati F, Yavuz F, Asadi H, Richards J P, Jourdan F (2013). Petrology and geochemistry of calc–alkaline volcanic and subvolcanic rocks, Dalli porphyry copper–gold deposit, Markazi Province, Iran. Int Geol Rev, 55(2): 158–184

Bai J, Porwal A, Hart C, Ford A, Yu L (2010). Mapping geochemical singularity using multifractal analysis: application to anomaly definition on stream sediments data from Funin Sheet, Yunnan, China. J Geochem Explor, 104(1–2): 1–11

Boomeri M, Nakashima K, Lentz D R (2009). The Miduk porphyry Cu deposit, Kerman, Iran: a geochemical analysis of the potassic zone including halogen element systematics related to Cu mineralization processes. J Geochem Explor, 103(1): 17–29

Bonham-Carter G F (1994). Geographic Information Systems for Geoscientists, Modelling with GIS. Pergamon: Oxford

Buccianti A (2015). The FOREGS repository: modelling variability in stream water on a continental scale revising classical diagrams from CoDA (compositional data analysis) perspective. J Geochem Explor, 154: 94–104

Buccianti A, Lima A, Albanese S, De Vivo B (2018). Measuring the change under compositional data analysis (CoDA): insight on the dynamics of geochemical systems. J Geochem Explor, 189: 100–108

Carranza E J M (2008). Geochemical anomaly and mineral prospectivity mapping in GIS. Handbook of Exploration and Environmental Geochemistry, 11

Carranza E J M (2009). Objective selection of suitable unit cell size in data-driven modeling of mineral prospectivity. Comput Geosci, 35 (10): 2032–2046

Carranza E J M (2011). Analysis and mapping of geochemical anomalies using logratio-transformed stream sediment data with censored values. J Geochem Explor, 110(2): 167–185

Carranza E J M, Hale M (1997). A catchment basin approach to the analysis of reconnaissance geochemical-geological data from Albay Province, Philippines. J Geochem Explor, 60(2): 157–171

Chaffee M A, Hill R H, Sutley S J, Watterson J R (1981). Regional geochemical studies in the Patagonia Mountains, Santa Cruz County, Arizona. J Geochem Explor, 14: 135–153

Chen Y, Lu L, Li X (2014). Application of continuous restricted Boltzmann machine to identify multivariate geochemical anomaly. J Geochem Explor, 140: 56–63

Cheng Q (1999). Spatial and scaling modelling for geochemical anomaly separation. J Geochem Explor, 65(3): 175–194

Cheng Q (2007). Mapping singularities with stream sediment geochemical data for prediction of undiscovered mineral deposits in Gejiu, Yunnan Province, China. Ore Geol Rev, 32(1–2): 314–324

Cheng Q, Agterberg F P (2009). Singularity analysis of ore-mineral and toxic trace elements in stream sediments. Comput Geosci, 35(2): 234–244

Cheng Q, Agterberg F P, Ballantyne S B (1994). The separation of geochemical anomalies from background by fractal methods. J Geochem Explor, 51(2): 109–130

Cheng Q, Agterberg F P, Bonham-Carter G F (1996). A spatial analysis method for geochemical anomaly separation. J Geochem Explor, 56 (3): 183–195

Cheng Q, Xu Y, Grunsky E (2000). Integrated spatial and spectrum method for geochemical anomaly separation. Nat Resour Res, 9(1): 43–52

Cheng Q, Jing L, Panahi A (2006). Principal component analysis with optimum order sample correlation coefficient for image enhancement. Int J Remote Sens, 27(16): 3387–3401

Cheng Q, Bonham-Carter G, Wang W, Zhang S, Li W, Qinglin X (2011). A spatially weighted principal component analysis for multi-element geochemical data for mapping locations of felsic intrusions in the Gejiu mineral district of Yunnan, China. Comput Geosci, 37(5): 662–669

Cohen D R, Kelley D L, Anand R, Coker W B (2010). Major advances in exploration geochemistry, 1998–2007. Geochem Explor Environ Anal, 10(1): 3–16

Darabi-Golestan F, Hezarkhani A (2019). Applied statistical functions and multivariate analysis of geochemical compositional data to evaluate mineralization in Glojeh polymetallic deposit, NW Iran. Front Earth Sci-PRC, 13(1): 229–246

Andrada de Palomera P, van Ruitenbeek F J A, Carranza E J M (2015). Prospectivity for epithermal gold–silver deposits in the Deseado Massif, Argentina. Ore Geol Rev, 71: 484–501

Rocha W F C, Nogueira R, Baptista da Silva G E, Queiroz S M, Sarmanho G F (2013). A comparison of three procedures for robust PCA of experimental results of the homogeneity test of a new sodium diclofenac candidate certified reference material. Microchem J, 109: 112–116

Dimitrijevic M D (1973). Geology of Kerman Region. Geological Survey of Iran Report YU/52

Egozcue J J, Pawlowsky-Glahn V, Mateu-Figueras G, Barceloó-Vidal C (2003). Isometric logratio transformations for compositional data analysis. Math Geol, 35(3): 279–300

Filzmoser P, Hron K (2008). Outlier detection for compositional data using robust methods. Math Geosci, 40(3): 233–248

Filzmoser P, Hron K (2009). Correlation analysis for compositional data. Math Geosci, 41(8): 905–919

Filzmoser P, Hron K, Reimann C (2009a). Principal component analysis for compositional data with outliers. Environmetrics, 20(6): 621–632

Filzmoser P, Hron K, Reimann C, Garrett R (2009b). Robust factor analysis for compositional data. Comput Geosci, 35(9): 1854–1861

Ghasemzadeh S, Maghsoudi A, Yousefi M, Mihalasky M J (2019a). Stream sediment geochemical data analysis for district-scale mineral exploration targeting: Measuring the performance of the spatial U-statistic and C-A fractal modeling. Ore Geol Rev, 113: 103115

Ghasemzadeh S, Maghsoudi A, Yousefi M (2019b). Application of geometric average approach for Cu-porphyry prospectivity mapping in the Baft area, Kerman. J Geosci (Prague), 29: 123–130

Gong Q, Li J, Xiang Y, Liu R, Wu X, Yan T, Chen J, Li R, Tong Y (2018). Determination and classification of geochemical anomalies based on backgrounds and cutoff grades of trace elements: a case study in South Nanling Range, China. J Geochem Explor, 194: 44–51

Grunsky E C, Drew L J, Sutphin D M (2009). Process recognition in multi-element soil and stream-sediment geochemical data. Appl Geochem, 24(8): 1602–1616

Halter W E, Bain N, Becker K, Heinrich C A, Landtwing M, VonQuadt A, Clark A H, Sasso A M, Bissig T, Tosdal R M (2004). From andesitic volcanism to the formation of a porphyry Cu-Au mineralizing magma chamber: the Farallo'n Negro Volcanic Complex, northwestern Argentina. J Volcanol Geotherm Res, 136(1–2): 1–30

Harris J R, Wilkinson L, Grunsky E C (2000). Effective use and interpretation of lithogeochemical data in regional mineral exploration programs: application of Geographic Information Systems (GIS) technology. Ore Geol Rev, 16(3–4): 107–143

He J Z, Yao S Z, Zhang Z P, You G J (2013). Complexity and productivity differentiation models of metallogenic indicator elements in rocks and supergene media around Daijiazhuang Pb–Zn deposit in Dangchang County, Gansu Province. Nat Resour Res, 22 (1): 19–36

Hezarkhani A (2006). Petrology of the intrusive rocks within the Sungun Porphyry Copper Deposit, Azerbaijan, Iran. J Asian Earth Sci, 27(3): 326–340

Hezarkhani A, Williams-Jones A E (1998). Controls of alteration and mineralization in the Sungun porphyry copper deposit, Iran; evidence from fluid inclusions and stable isotopes. Econ Geol, 93(5): 651–670

Hengl T (2006). Finding the right pixel size. Comput Geosci, 32(9): 1283–1298

Hurst H E (1951). Long-term storage capacity of reservoirs. Trans Am Soc Civ Eng, 116: 770–808

Jamali H (2017). The behavior of rare-earth elements, zirconium and hafnium during magma evolution and their application in determining mineralized magmatic suites in subduction zones: constraints from the Cenozoic belts of Iran. Ore Geol Rev, 81: 270–279

John D A, Ayuso R A, Barton M D, Blakely R J, Bodnar R J, Dilles J H, Gray F, Graybeal F T, Mars J C, McPhee D K, Seal R R, Taylor R D, Vikre P G (2010). Porphyry Copper Deposit Model: Chapter B in Mineral Deposit Models for Resource Assessment. Reston: U.S. Geological Survey

Jolliffe I (2002). Principal Component Analysis and Factor Analysis. Principal Component Analysis. New York: Springer

Kirkwood C, Cave M, Beamish D, Grebby S, Ferreira A (2016). A machine learning approach to geochemical mapping. J Geochem Explor, 167: 49–61

Kreuzer O P, Yousefi M, Nykänen V (2020). Introduction to the special issue on spatial modelling and analysis of ore forming processes in mineral exploration targeting. Ore Geol Rev, 119: 103391

Li C, Ma T, Shi J (2003). Application of a fractal method relating concentrations and distances for separation of geochemical anomalies from background. J Geochem Explor, 77(2–3): 167–175

Macklin M G, Ridgway J, Passmore D G, Rumsby B T (1994). The use of overbank sediment for geochemical mapping and contamination assessment: results from selected English and Welsh floodplains. Appl Geochem, 9(6): 689–700

Mandelbrot B B, Wallis J R (1969). Some long-run properties of geographysical records. Water Resour Res, 5(2): 321–340

Mirzaie A, Bafti S S, Derakhshani R (2015). Fault control on Cu mineralization in the Kerman porphyry copper belt, SE Iran: a fractal analysis. Ore Geol Rev, 71: 237–247

Mohajjel M, Fergusson C L (2000). Dextral transpression in Late Cretaceous continental collision, Sanandaj–Sirjan zone, western Iran. J Struct Geol, 22(8): 1125–1139

Moon C J (1999). Towards a quantitative model of downstream dilution of point source geochemical anomalies. J Geochem Explor, 65(2): 111–132

Moghadam M C, Tahmasbi Z, Ahmadi-Khalaji A, Santos J F (2018). Petrogenesis of Rabor-Lalehzar magmatic rocks (SE Iran): constraints from whole rock chemistry and Sr-Ndisotopes. Geochemistry, 78(1): 58–77

Niktabar S M, Moradian A, Ahmadipour H, Santos J F, Mendes M H (2015). Petrogenesis of the Lalezar granitoid intrusions (Kerman Province-Iran). Journal of Sciences, 26(4): 333–348

Parsa M, Maghsoudi A, Yousefi M, Sadeghi M (2016). Prospectivity modeling of porphyry-Cu deposits by identification and integration of efficient mono-elemental geochemical signatures. J Afr Earth Sci, 114: 228–241

Parsa M, Maghsoudi A, Carranza E J M, Yousefi M (2017 a). Enhancement and mapping of weak multivariate stream sediment geochemical anomalies in Ahar Area, NW Iran. Nat Resour Res, 26 (4): 443–455

Parsa M, Maghsoudi A, Yousefi M (2017 b). An improved data-driven fuzzy mineral prospectivity mapping procedure; cosine amplitude-based similarity approach to delineate exploration targets. Int J Appl Earth Obs Geoinf, 58: 157–167

Parsa M, Maghsoudi A, Yousefi M (2018a). A receiver operating characteristics-based geochemical data fusion technique for targeting undiscovered mineral deposits. Nat Resour Res, 27(1): 15–28

Parsa M, Maghsoudi A, Yousefi M (2018b). Spatial analyses of exploration evidence data to model skarn-type copper prospectivity in the Varzaghan district. NW Iran. Ore Geol Rev, 92: 97–112

Pirajno F (2010). Intracontinental strike-slip faults, associated magmatism, mineral systems and mantle dynamics: examples from NW China and Altay-Sayan (Siberia). J Geodyn, 50(3–4): 325–346

Pison G, Rousseeuw P J, Filzmoser P, Croux C (2003). Robust factor analysis. J Multivariate Anal, 84(1): 145–172

Peytcheva I, von Quadt A, Neubauer F, Frank M, Nedialkov R, Heinrich C, Strashimirov S (2009). U–Pb dating, Hf-isotope characteristics and trace-REE-patterns of zircons from Medet porphyry copper deposit, Bulgaria: implications for timing, duration and sources of ore-bearing magmatism. Miner Petrol, 96(1–2): 19–41

Qu X, Hou Z, Zaw K, Li Y (2007). Characteristics and genesis of Gangdese porphyry copper deposits in the southern Tibetan Plateau: Preliminary geochemical and geochronological results. Ore Geol Rev, 31(1–4): 205–223

Reimann C, Filzmoser P (2000). Normal and lognormal data distribution in geochemistry: death of a myth. Consequences for the statistical treatment of geochemical and environmental data. Environ. Geol., 39

(9): 1001–1014

Reimann C, Filzmoser P, Garrett R G (2002). Factor analysis applied to regional geochemical data: problems and possibilities. Appl Geochem, 17(3): 185–206

Rezaei-Kahkhaei M, Galindo C, Pankhurst R J, Esmaeily D (2011). Magmatic differentiation in the calc-alkaline Khalkhab–Neshveh pluton, Central Iran. J Asian Earth Sci, 42(3): 499–514

Rousseeuw P J, Driessen K V (1999). A fast algorithm for the minimum covariance determinant estimator. Technometrics, 41(3): 212–223

Shafiei B, Haschke M, Shahabpour J (2009). Recycling of orogenic arc crust triggers porphyry Cu mineralization in Kerman Cenozoic arc rocks, southeastern Iran. Miner Depos, 44(3): 265–283

Shafiei B (2010). Lead isotope signatures of the igneous rocks and porphyry copper deposits from the Kerman Cenozoic magmatic arc (SE Iran), and their magmatic-metallogenetic implications. Ore Geol Rev, 38(1–2): 27–36

Soltani F, Moarefvand P, Alinia F, Afzal P (2019). Characterization of rare earth elements by coupling multivariate analysis, factor analysis, and geostatistical simulation: case-study of Gazestan deposit, central Iran. J Min Environ, 10(4): 929–945

Sillitoe R H (1972). A plate tectonic model for the origin of porphyry copper deposits. Econ Geol, 67(2): 184–197

Sillitoe R H (2010). Porphyry copper systems. Econ Geol, 105(1): 3–41

Singer D A, Berger V I, Moring B C (2005). Porphyry Copper Deposits of the World: Database, Maps, Grade and Tonnage Models. Reston: US Department of the Interior, US Geological Survey,1005–1060

Spadoni M (2006). Geochemical mapping using a geomorphologic approach based on catchments. J Geochem Explor, 90(3): 183–196

Spadoni M, Voltaggio M, Cavarretta G (2005). Recognition of areas of anomalous concentration of potentially hazardous elements by means of a subcatchment-based discriminant analysis of stream sediments. J Geochem Explor, 87(3): 83–91

Srdic A, Dimitrijevic M N, Cvetic S, Dimitrijevic M D (1972). Geological Map of Baft (1: 100,000). Teheran: Geological Survey of Iran Publication

Templ M, Hron K, Filzmoser P (2011). robCompositions: an R-package for robust statistical analysis of compositional data. In: Pawlowsky-Glahn V, Buccianti A, eds. Compositional Data Analysis: Theory and Applications. Chichester: Wiley, 341–355

Tian M, Wang X, Nie L, Zhang C (2018). Recognition of geochemical anomalies based on geographically weighted regression: a case study across the boundary areas of China and Mongolia. J Geochem Explor, 190: 381–389

Thompson M, Howarth R J (1976). Duplicate analysis in geochemical practice. Part 1: theoretical approach and estimation of analytical reproducibility. Analyst (Lond), 101(1206): 690–698

Wang H, Zuo R (2015). A comparative study of trend surface analysis and spectrum–area multifractal model to identify geochemical anomalies. J Geochem Explor, 155: 84–90

Wang H, Cheng Q, Zuo R (2015). Quantifying the spatial characteristics of geochemical patterns via GIS-based geographically weighted statistics. J Geochem Explor, 157: 110–119

Wang J, Zuo R (2016). An extended local gap statistic for identifying geochemical anomalies. J Geochem Explor, 164: 86–93

Wang J, Zuo R, Caers J (2017). Discovering geochemical patterns by factor-based cluster analysis. J Geochem Explor, 181: 106–115

Wang J, Zhou Y, Xiao F (2020). Identification of multi-element geochemical anomalies using unsupervised machine learning algorithms: a case study from Ag-Pb-Zn deposits in north-western Zhejiang, China. Appl Geochem: 104679

Wang Z, Dong Y, Zuo R (2019). Mapping geochemical anomalies related to Fe–polymetallic mineralization using the maximum margin metric learning method. Ore Geol Rev, 107: 258–265

Xiao F, Chen J, Zhang Z, Wang C, Wu G, Agterberg F P (2012). Singularity mapping and spatially weighted principal component analysis to identify geochemical anomalies associated with Ag and Pb-Zn polymetallic mineralization in northwest Zhejiang, China. J Geochem Explor, 122: 90–100

Xiao F, Wang K, Hou W, Erten O (2020). Identifying geochemical anomaly through spatially anisotropic singularity mapping: a case study from silver-gold deposit in Pangxidong district, SE China. J Geochem Explor, 210: 106453

Xie X, Wang X, Zhang Q, Zhou G, Cheng H, Liu D, Cheng Z, Xu S (2008). Multi-scale geochemical mapping in China. Geochem Explor Environ Anal, 8(3–4): 333–341

Xie S, Cheng Q, Xing X, Bao Z, Chen Z (2010). Geochemical multifractal distribution patterns in sediments from ordered streams. Geoderma, 160(1): 36–46

Xiong Y, Zuo R, Wang K, Wang J (2018). Identification of geochemical anomalies via local RX anomaly detector. J Geochem Explor, 189: 64–71

Xiong Y, Zuo R (2020). Recognizing multivariate geochemical anomalies for mineral exploration by combining deep learning and one-class support vector machine1. Comput Geosci, 140: 104484

Yang Z, Hou Z, White N C, Chang Z, Li Z, Song Y (2009). Geology of the post-collisional porphyry copper–molybdenum deposit at Qulong, Tibet. Ore Geol Rev, 36(1–3): 133–159

Yilmaz H (2003a). Exploration at the Kuscayiri Au (Cu) prospect and its implications for porphyry-related mineralization in western Turkey. J Geochem Explor, 77(2–3): 133–150

Yilmaz H (2003b). Geochemical exploration for gold in western Turkey: success and failure. J Geochem Explor, 80(1): 117–135

Yousefi M (2017a). Recognition of an enhanced multi-element geochemical signature of porphyry copper deposits for vectoring into mineralized zones and delimiting exploration targets in Jiroft area, SE Iran. Ore Geol Rev, 83: 200–214

Yousefi M (2017b). Analysis of zoning pattern of geochemical indicators for targeting of porphyry-Cu mineralization: a pixel-based mapping approach. Nat Resour Res, 26(4): 429–441

Yousefi M, Carranza E J M (2015). Fuzzification of continuous-value spatial evidence for mineral prospectivity mapping. Comput Geosci, 74: 97–109

Yousefi M, Kamkar-Rouhani A, Carranza E J M (2012). Geochemical mineralization probability index (GMPI): a new approach to generate enhanced stream sediment geochemical evidential map for increasing probability of success in mineral potential mapping. J Geochem Explor, 115: 24–35

Yousefi M, Carranza E J M, Kamkar-Rouhani A (2013). Weighted drainage catchment basin mapping of geochemical anomalies using stream sediment data for mineral potential modeling. J Geochem Explor, 128: 88–96

Yousefi M, Kreuzer O P, Nykänen V, Hronsky J M (2019). Exploration

information systems-a proposal for the future use of GIS in mineral exploration targeting. Ore Geol Rev, 111: 103005

Yousefi M, Nykänen V (2017). Introduction to the special issue: GIS-based mineral potential targeting. J Afr Earth Sci (Paris), 128: 1–4

Yu X, Xiao F, Zhou Y, Wang Y, Wang K (2019). Application of hierarchical clustering, singularity mapping, and Kohonen neural network to identify Ag-Au-Pb-Zn polymetallic mineralization associated geochemical anomaly in Pangxidong district. J Geochem Explor, 203: 87–95

Zarasvandi A, Rezaei M, Sadeghi M, Lentz D, Adelpour M, Pourkaseb H (2015). Rare earth element signatures of economic and sub-economic porphyry copper systems in Urumieh–Dokhtar Magmatic Arc (UDMA), Iran. Ore Geol Rev, 70: 407–423

Zhao J, Wang W, Dong L, Yang W, Cheng Q (2012). Application of geochemical anomaly identification methods in mapping of intermediate and felsic igneous rocks in eastern Tianshan, China. J Geochem Explor, 122: 81–89

Zhou S, Zhou K, Cui Y, Wang J, Ding J (2015). Exploratory data analysis and singularity mapping in geochemical anomaly identification in Karamay, Xinjiang, China. J Geochem Explor, 154: 171–179

Zhao J, Chen S, Zuo R (2016). Identifying geochemical anomalies associated with Au–Cu mineralization using multifractal and artificial neural network models in the Ningqiang district, Shaanxi, China. J Geochem Explor, 164: 54–64

Zhang C, Jordan C, Higgins A (2007). Using neighbourhood statistics and GIS to quantify and visualize spatial variation in geochemical variables: an example using Ni concentrations in the top soils of Northern Ireland. Geoderma, 137(3–4): 466–476

Zhou S, Zhou K, Wang J, Yang G, Wang S (2018). Application of cluster analysis to geochemical compositional data for identifying ore-related geochemical anomalies. Front Earth Sci, 12(3): 491–505

Zheng Y, Sun X, Gao S, Wang C, Zhao Z, Wu S, Li J, Wu X (2014). Analysis of stream sediment data for exploring the Zhunuo porphyry Cu deposit, southern Tibet. J Geochem Explor, 143: 19–30

Zuo R (2011). Identifying geochemical anomalies associated with Cu and Pb–Zn skarn mineralization using principal component analysis and spectrum–area fractal modeling in the Gangdese Belt, Tibet (China). J Geochem Explor, 111(1–2): 13–22

Zuo R (2012). Exploring the effects of cell size in geochemical mapping. J Geochem Explor, 112: 357–367

Zuo R (2014). Identification of weak geochemical anomalies using robust neighborhood statistics coupled with GIS in covered areas. J Geochem Explor, 136: 93–101

Zuo R (2017). Machine learning of mineralization-related geochemical anomalies: a review of potential methods. Nat Resour Res, 26(4): 457–464

Zuo R, Xiong Y (2020). Geodata science and geochemical mapping. J Geochem Explor, 209: 106431

Zuo R, Cheng Q, Agterberg F P, Xia Q (2009a). Application of singularity mapping technique to identify local anomalies using stream sediment geochemical data, a case study from Gangdese, Tibet, western China. J Geochem Explor, 101(3): 225–235

Zuo R, Cheng Q, Xia Q (2009b). Application of fractal models to characterization of vertical distribution of geochemical element concentration. J Geochem Explor, 102(1): 37–43

Zuo R, Xia Q, Wang H (2013). Compositional data analysis in the study of integrated geochemical anomalies associated with mineralization. Appl Geochem, 28: 202–211

Zuo R, Wang J (2016). Fractal/multifractal modeling of geochemical data: a review. J Geochem Explor, 164: 33–41